Low-energy positron interactions with xenon

2011 New J. Phys. 13 125004

(http://iopscience.iop.org/1367-2630/13/12/125004)

New Journal of Physics
The open-access journal for physics

Low-energy positron interactions with xenon

J R Machacek[1], C Makochekanwa[1], A C L Jones[1,6], P Caradonna[1,7], D S Slaughter[1,8], R P McEachran[1], J P Sullivan[1], S J Buckman[1,9], S Bellm[2], B Lohmann[2], D V Fursa[3], I Bray[3], D W Mueller[4] and A D Stauffer[5]

[1] ARC Centre for Antimatter-Matter Studies, Research School of Physics and Engineering, Australian National University, Canberra, ACT 0200, Australia
[2] ARC Centre for Antimatter-Matter Studies, The University of Adelaide, Adelaide, SA, Australia
[3] ARC Centre for Antimatter-Matter Studies, Curtin University of Technology, GPO Box U1987, Perth, WA 6845, Australia
[4] Physics Department, University of North Texas, Denton, TX, USA
[5] Department of Physics and Astronomy, York University, Toronto, Canada
E-mail: Stephen.Buckman@anu.edu.au

New Journal of Physics **13** (2011) 125004 (19pp)
Received 3 August 2011
Published 8 December 2011
Online at http://www.njp.org/
doi:10.1088/1367-2630/13/12/125004

Abstract. Low-energy interactions of positrons with xenon have been studied both experimentally and theoretically. The experimental measurements were carried out using a trap-based positron beam with an energy resolution of ∼80 meV, while the theoretical calculations were carried out using the convergent close-coupling method and the relativistic optical potential approach. Absolute values of the grand total, positronium formation and grand total minus positronium formation cross sections are presented over the energy range of 1–60 eV. Elastic differential cross sections (DCS), for selected energies, are also presented both below and above the positronium formation threshold. Fine energy-step measurements of the positronium formation cross section over the energy range of 4.4–8.4 eV, and measurements of the elastic DCS at the energies of 5.33 and 6.64 eV, have been carried out to investigate the ionization threshold

[6] Present address: Physics Department, University of California San Diego, San Diego, CA, USA.
[7] Present address: Max Planck Institute, Heidelberg, Germany.
[8] Present address: Lawrence Berkeley Laboratory, Berkeley, CA, USA.
[9] Author to whom any correspondence should be addressed.

regions corresponding to the $^2P_{3/2}$ and $^2P_{1/2}$ states of the Xe^+ ion. The present results are compared with both experimental and theoretical values from the literature where available.

Contents

1. Introduction

Compared with electron scattering, where high-resolution state-resolved cross sections have been achieved and benchmarked experimentally for about 20 years (see, e.g., [1, 2] and references therein), experimental studies of positron scattering from atoms and molecules have been less extensive and less sophisticated. This is due, in part, to the difficulties involved in creating the sufficiently monoenergetic and intense beams of positrons required for such measurements. However, with the recent development of efficient positron traps, trap-based beams and new techniques for studying positron scattering in a high magnetic field [3–5], it is now possible to carry out measurements that were previously not possible. From a theoretical perspective, the advances that have been made in electron scattering calculations have not been reproduced to the same level for positron scattering, due in large part to the complication arising from inclusion of the additional channel of positronium (Ps) formation. These differences in the quality and accuracy of electron and positron scattering data are still broadly evident in most atomic and molecular systems, and xenon is an interesting case in point. Examination of the literature reveals a large spread, for example, in the experimental and theoretical values for even the most straightforward measurement of the total scattering cross section.

This paper represents part of our group's broader drive to develop data sets with which we can hopefully benchmark experiment and theory for positron scattering from the noble gases. To date, studies have been conducted on low-energy positron scattering from helium, neon (Ne), argon (Ar) and krypton (Kr). For helium, the grand total (σ_{GT}), Ps formation (σ_{Ps}) and grand total minus Ps formation (σ_{GT}–σ_{Ps}) have been studied [6–8] as well as electronic excitation (σ_{Exc}) cross sections [8, 9]. σ_{GT}, σ_{Ps} and σ_{GT}–σ_{Ps} have also been studied for Ne and Ar [10],

while these three cross sections as well as elastic differential cross sections (DCS) have also been studied for Kr [11]. The present work on xenon (Xe) completes this suite of measurements and calculations on the family of noble gases.

As was the case for other noble gases, there are a reasonable number of experimental and theoretical data available for σ_{GT} and σ_{Ps} in the literature for Xe, albeit characterized by the significant differences in magnitude and energy dependence alluded to above. Most of the available data in the literature for σ_{GT} are from the 1970s and 1980s, and have been well summarized up to 1992 by Baluja and Jain [12]. The only work since has been the semi-empirical theoretical estimation by Parcell *et al* [13]. The experimental results for σ_{Ps} from this target have been well summarized by Marler *et al* [14], while the current state of the theoretical calculations for this cross section was presented very recently by Gilmore *et al* [15]. Elastic DCS data also exist in the literature for Xe. These consist of a set of absolute measurements [16], at three energies, and one set of relative measurements [17], as well as two theoretical calculations [18, 19].

In the following sections, we briefly discuss the experimental techniques and theoretical approaches that have been applied in this work and we present the results for these cross sections in comparison with the values from the literature where available.

2. Experimental apparatus and procedures

The measurements presented here were carried out using a Surko trap-based experimental apparatus [3, 4]. This has been comprehensively described elsewhere [20], so only a brief overview of the operation will be presented here. Positrons are obtained from a radioactive source of ^{22}Na which had an activity of approximately 40 mCi for the measurements presented in this paper. A solid Ne moderator is used to form a low-energy positron beam, which is radially confined using solenoidal magnetic fields (∼100 G), and transported into a three-stage buffer-gas trap where the field is 530 G. The trap electrodes form a stepped electrostatic potential well, and positrons lose energy inside the trap through inelastic collisions with a mixture of N_2 and CF_4 buffer gases, in the process thermalizing to room temperature. This trapped cloud of positrons becomes the reservoir for a pulsed positron beam. Trap operation is typically cycled at approximately 100–200 Hz with up to 1000 positrons per pulse. Careful control over the beam formation means that the energy width of the beam is comparable with the temperature of the trapped positron cloud. In these experiments, the typical energy resolution was ∼80 meV.

The positron beam is directed to a gas cell; the gas cell is 100 mm in length, with 5 mm diameter entrance and exit apertures, and contains the Xe target gas. The potential of the gas cell defines the energy of the positrons within the cell and the target gas is well localized to 100 mm path length. The target density inside the cell is maintained so that total positron scattering is not more than 10% of the unscattered beam, in order to avoid multiple scattering effects. Most of the positrons are transmitted through the gas cell and pass through a retarding potential analyzer (RPA), which is sensitive only to the parallel energy component of the beam ($E_\parallel$). Those that are transmitted by the RPA are then detected by a micro-channel plate detector. In a collision with a target atom, the positron can be scattered through some angle θ, in the process losing some $E_\parallel$, and it can also lose some of its total energy if inelastic processes are energetically allowed [5]. Ps formation is also possible above the Ps formation threshold, E_{Ps}, corresponding to 5.33 eV for Xe, and results in a loss of positrons from the transmitted beam and thus a loss of observed positron intensity at the detector.

In our experimental approach, the zero for the energy scale is established with a retarding potential analysis of the beam, i.e. with the energy scale defined relative to the 'cut-off' position of the beam. This procedure results in an uncertainty of ± 20 meV in the energy scale. The scattering cell target pressure was measured using a model 690 MKS Baratron capacitance manometer with a full range of 1 torr and a measurement accuracy of about 5% for the low pressure range that was required for these measurements, in order to maintain the total scattering fraction below 10%. There are a number of possible sources of systematic error in our measurements and these have been estimated and accounted for, where possible, and have been discussed previously [20]. For these experiments, statistical errors are typically less than 3% for the total scattering and less than 10% for the Ps formation measurements, whereas for the differential elastic measurements they can be significantly larger (5–10%). Total systematic effects typically account for an uncertainty of about 7%. Thus the total uncertainties in σ_{GT} and σ_{Ps} are in the range of 7–9%, while those for the DCS measurements are typically between 9 and 17%, with the values shown in the tables that follow.

2.1. Total cross section measurements

The techniques that have been used for the measurement of σ_{GT}, σ_{Ps} and σ_{GT}–σ_{Ps} have been presented in recent papers [10, 21] and will not be repeated in detail here. The basic technique is a variation of the Beer–Lambert law, where scattering is equated to the loss of parallel energy in the magnetic field. Absolute cross sections can be obtained using the measured gas pressure and scattering cell length.

As with any transmission experiment using a scattering cell, our experimental technique has some angular discrimination limitations. This arises from the inability to distinguish between positrons that are elastically scattered at small angles from those in the primary, unscattered beam. This issue always results in the directly measured total and total elastic cross sections being smaller than the 'true' values. The extent of the problem depends on the angular discrimination of the apparatus and the nature of the differential elastic scattering cross section in this forward angle region. It has been discussed in detail in a recent publication [21].

From the knowledge of our apparatus' angular discrimination and using the elastic DCS either measured and/or calculated in this work, we can make a reasonable estimate of the contribution to the total cross section that is missing from our measured cross section. Note that this forward scattering problem only affects those positrons elastically scattered into this experimentally inaccessible angular range $(0 \pm \theta_c)$, where θ_c is the smallest scattering angle effectively discriminated against in the experiment. Note also that the correction only to be applied only for the measured σ_{GT} and σ_{GT}–σ_{Ps} and not for σ_{Ps}.

Using the elastic DCS calculated from the present relativistic optical potential (ROP) approach, and the method and equations discussed previously [5, 10, 21], we have estimated the correction that needs to be applied to the measured cross sections at each energy to account for this missing angular range. The results are shown in table 1.

2.2. Elastic differential cross sections

Once again, the techniques used for the measurements of the elastic DCS, below and above the threshold for Ps formation, have been presented in a recent paper [11], while the details of the data analysis, and the limitations of this technique, have been discussed elsewhere [5, 22], so we will not be repeating that detail here. In short, these techniques make use of

Table 1. Estimated missing angular range (θ_c) and the corresponding corrections to σ_{GT} and σ_{GT}–σ_{Ps} for selected positron scattering energies.

Energy (eV)	θ_c	Correction (%)
0.5	27	20
1.0	18	18
2.0	13	14
5.0	8	10
8.0	6	7

the principles of positron motion and scattering in a strong magnetic field, along with the same experimental techniques used for the total cross section measurements described above. As highlighted above, the RPA analyses only the parallel energy component of the positron beam ($E_\parallel$) and the transmitted current, I, as a function of $E_\parallel$ can be related to the differential scattering cross section (below any inelastic thresholds) through the relationship

$$\frac{d\sigma}{d\Omega} = \frac{\sqrt{E_\parallel E}}{\pi n \ell I_0}\left(\frac{dI_c(E)}{dE_\parallel}\right), \tag{1}$$

where n is the number density of the target gas in the scattering cell, l is the length of the scattering cell, I_0 is the incident positron intensity and I_c is the transmitted positron intensity as a function of the scattering energy E. All positrons that are scattered in the cell travel through to the RPA and those with $E_\parallel$ greater than the RPA potential pass through to the detector. As with the total cross section measurements, the scattering probability on a single pass through the cell must be adjusted so that there is a small chance of re-scattering. That is, the total scattering probabilities for these measurements are also kept at less than 10%, and the cross sections are checked to ensure that there is no pressure dependence.

We also note that positrons that are scattered in the backwards direction (i.e. through angles greater than 90°) can be reflected from the potential barriers associated with the trap and other elements and can travel back through the gas cell. The result of this backward scattered contribution is that the measured cross section at any angle θ actually consists of contributions from scattering through θ and 180–θ; that is, the cross section is 'folded' around 90° [5]. This has to be taken into account when making comparisons with theory.

In this paper, we also present measurements of the elastic DCS at energies above the first inelastic excitation threshold, and this requires an alteration of the experimental technique from that described above for the case of pure elastic scattering. This is a result of the need to separate those positrons scattered elastically from those that have undergone inelastic scattering. Details of the technique we use to achieve this have been described for measurements of electronic excitation cross sections [9] and also in [5]. Briefly, this makes use of the fact that for a slowly varying magnetic field, the magnetic moment of a charged particle, the ratio of the perpendicular energy component of the positron beam to the magnetic field ($E_\perp/B$), is an adiabatic invariant. As a result, by changing the ratio of the field in the scattering cell (B_{SC}) to that at the RPA (B_{RPA}), i.e. $M = B_{SC}/B_{RPA}$, this invariant quantity can be used to our advantage. Depending on the magnitude of M, this technique enables us to convert some, or all, of the positron's perpendicular energy, arising as a result of angular scattering, back into the parallel component. This way we can separate losses of total energy due to excitation processes from those due to angular elastic scattering. For the present measurements of above threshold elastic scattering, we

used $M = 3$, allowing the elastic DCS to be measured at energies up to the 20 eV data presented in this paper.

3. Theoretical procedures

We employ two theoretical treatments to compute cross sections for positron scattering from Xe. One is an ROP calculation [23], which has been used to calculate the grand total cross section (σ_{GT}) below E_{Ps} and the grand total minus Ps formation (σ_{GT}–σ_{Ps}) above E_{Ps}. The other approach is the convergent close-coupling (CCC) technique [24] and is a calculation of σ_{GT} at all energies. Both techniques have recently been discussed in detail [10, 11] and only a brief description is given here.

3.1. The relativistic optical potential method

The theoretical cross sections presented here for Xe were determined from the solution of the relativistic Dirac–Fock scattering equations containing static, polarization and *ab initio* complex optical potentials. The details of this method have been given in [23] and its application to positron scattering from Ne and Ar is discussed in [10]. Thus, only a brief discussion of its application to Xe is given here.

In the case of Xe, the dipole and the next four higher multipoles were included in the polarization potential. Whenever the energy of the incident positron was such that inelastic channels (excitation and ionization) were open, the imaginary part of the optical potential was incorporated to describe absorption processes. This absorption potential is both non-local and *ab initio* and is determined as an expansion over the inelastic channels of the target, which include both excitation of the discrete bound states and single ionization of the target.

The discrete Dirac–Fock wavefunctions of the target were determined using the multi-configuration Dirac–Fock (MCDF) program of Grant *et al* [25]. Here the absorption potential included the following 15 excited states (in intermediate coupling notation):

$$5\bar{d}[1/2]^0_{J=1} \quad 5d[3/2]^0_{J=1} \quad 5\bar{d}[3/2]^0_{J=1} \quad 5d[7/2]^0_{J=3},$$
$$5\bar{d}[5/2]^0_{J=3} \quad 5d[5/2]^0_{J=3} \quad 6s[3/2]^0_{J=1} \quad 6s[1/2]^0_{J=1},$$
$$6p[1/2]_{J=0} \quad 6\bar{\mathrm{p}}[1/2]_{J=0} \quad 6\bar{\mathrm{p}}[5/2]_{J=2} \quad 6\bar{\mathrm{p}}[3/2]_{J=2},$$
$$6p[3/2]_{J=2} \quad 7s[3/2]^0_{J=1} \quad 7s[1/2]^0_{J=1}.$$

Here J represents the total angular momentum of the atom, while $\bar{p}$ represents a p-orbital with $j = 1/2$ and p represents a p-orbital with $j = 3/2$. Similarly, $\bar{d}$, d represent d-orbitals with $j = 3/2$, $5/2$, respectively. In addition, the absorption potential included the following continuum states:

$$\varepsilon s[3/2]^0_{J=1} \quad \varepsilon s[1/2]^0_{J=1} \quad \varepsilon p[1/2]_{J=0} \quad \varepsilon \bar{p}[1/2]_{J=0},$$
$$\varepsilon p[5/2]_{J=2} \quad \varepsilon p[3/2]_{J=2} \quad \varepsilon \bar{p}[3/2]_{J=2} \quad \varepsilon \bar{\mathrm{d}}[1/2]^0_{J=1},$$
$$\varepsilon \mathrm{d}[3/2]^0_{J=1} \quad \varepsilon \bar{\mathrm{d}}[3/2]^0_{J=1} \quad \varepsilon \mathrm{d}[7/2]^0_{J=3} \quad \varepsilon \mathrm{d}[5/2]^0_{J=3},$$
$$\varepsilon \bar{\mathrm{d}}[5/2]^0_{J=3} \quad \varepsilon s[1/2]_{J=0} \quad \varepsilon p[3/2]^0_{J=1} \quad \varepsilon \bar{p}[1/2]^0_{J=1},$$
$$\varepsilon d[5/2]_{J=2} \quad \varepsilon \bar{d}[3/2]_{J=2},$$

where ε represents the energy of the ejected electron, originally either a bound $5\bar{p}$ or $5p$ electron and, above 23.3 eV, a 5s electron.

Above the inelastic threshold, the scattering phase shifts are complex, i.e.

$$\eta_l^{\pm} = \delta_l^{\pm} + \mathrm{i}\gamma_l^{\pm}, \tag{2}$$

where the $\pm$ signs refer to a spin-up/spin-down positron. The elastic and inelastic cross sections are then determined from these phase shifts as described in [23].

3.2. The convergent close-coupling method

The CCC method solves the nonrelativistic Schrödinger equation for the positron–Xe scattering system by performing a close-coupling expansion of the total wavefunction in a basis of Xe atom target states. The resulting set of close-coupling equations is converted into the coupled Lippmann–Schwinger equations for the T-matrix, which are solved by standard techniques [26]. The target-state basis is obtained by diagonalization of the target Hamiltonian in a basis constructed from Sturmian (Laguerre) one-electron functions. The resulting basis provides a square-integrable representation for the target bound states and the continuum. The single-centered target state expansion used in the CCC method does not explicitly include Ps formation channels. However, outside the energy region between the Ps formation and direct ionization thresholds, they can be adequately represented due to completeness of the basis [10, 27, 28].

Calculation of Xe target states proceeds along the same scheme as that used recently for Ne and Ar [10] and Kr [11]. First we perform self-consistent Hartree–Fock calculations for the $Xe^+[Cd]5p^5$ ground state. Then, we conduct configuration interaction (CI) calculations by diagonalizing the Xe Hamiltonian in the basis of all possible $[Cd]5p^5\ nl$ configurations. The active electron is represented by the Laguerre basis [26] with basis size $N_l = 25 - l$ and exponential fall-off $\lambda_l = 3.0$ for $l \leqslant l_{\max} = 8$. This leads to 495 states in the close-coupling expansion. The accuracy of the present Xe structure model can be assessed by comparing the calculated ground state ionization energy, 11.74 eV, with the experimental value of 12.13 eV.

The total cross section calculated in the CCC method is affected by the value of the static dipole polarizability of the Xe atom. We have used a semi-empirical two-electron polarization potential [29] in order to bring the calculated static dipole polarizability close to its experimental value of 27.16 a.u. [30]. This potential modifies the dipole term of the positron–electron Coulomb potential and is given by the following expression:

$$V_p(r_0, r_i) = -\frac{\alpha}{r_0^3 r_i^3}(r_0 \bullet r_i)\sqrt{\left(1-\mathrm{e}^{-(r_0/\rho)^6}\right)\left(1-\mathrm{e}^{-(r_i/\rho)^6}\right)}, \tag{3}$$

where the index '0' refers to the positron and the index 'i' to one of the $Xe5p^6$ electrons. The parameters of the two-electron polarization potential are chosen to be $\alpha = 27.16$ a.u. and $\rho = 6.9$ a.u.

Finally, we note that Xe is a sufficiently heavy atom for which a relativistic approach is preferable. This is particularly important for excited states of Xe. However, for the elastic scattering cross section and aggregate observables such as the total cross section, the use of a nonrelativistic CCC approach is likely to be sufficient.

4. Results and discussion

In the discussion that follows, we present various total cross section (σ_{GT}, σ_{Ps} and σ_{GT}–σ_{Ps}) results and compare them with the data from the literature. The experimental data for these cross sections have been corrected for the angular discrimination limitations discussed earlier in section 2, using our elastic DCS calculated with the ROP method. Following this, we then discuss the results and calculations for the elastic DCS, and compare these with previous results where available.

4.1. Total cross sections

The numerical values for σ_{GT}, σ_{Ps} and σ_{GT}–σ_{Ps} are presented in table 2, and both experimental values and the current calculations are shown in figures 1 and 2, in comparison with the relevant values from the literature.

4.1.1. Grand total cross section (σ_{GT}). Figure 1(a) shows the present experimental and the CCC theoretical results for σ_{GT} and the results from the literature. The present experimental results are compared here with three other measurements [31–33], and they all largely agree with the present result with respect to the overall energy dependence of the cross section, although the magnitude varies significantly. The principal features are strong scattering at low energies ($\sim$30 Å^2 at 0.5 eV), which drops away smoothly until the Ps formation threshold, E_{Ps} ($\sim$15 Å^2 at 5.33 eV), above which the total cross section rises until 8 eV, beyond which it decreases slowly and monotonically until it is $\sim$15 Å^2 at 60 eV. Below 5.33 eV the scattering is purely elastic and the large low-energy cross section is driven mainly by polarization effects, the dipole polarizability of Xe being quite large at 27.16 a.u. The rapid rise above 5.33 eV is due to the opening up of the Ps formation channel, and is characteristic of the behavior in other atoms and molecules when this strong scattering channel is opened.

Perhaps the best agreement for σ_{GT} is found between the present experimental results and the measurements of Sinapius *et al* [31] over the whole energy range of overlap, i.e. 1–6 eV. The agreement is both in energy dependence and in magnitude. The experimental results of Coleman *et al* [32], although agreeing with the present results on the overall energy dependence, are less than the present values by more than a factor of 2 below E_{Ps} (5.33 eV), but rise sharply in magnitude to approach the present values at their highest energy point of 9 eV. The present results agree well with the results of Dababneh *et al* [33] on energy dependence over the entire energy range of overlap, but are, however, larger than the latter, e.g. they are $\sim$30% higher below E_{Ps}, are $\sim$50% higher at E_{Ps} and consistently $\sim$20% higher above E_{Ps}. In general, the present results are higher than all others at most energies below the Ps threshold and we have demonstrated in a previous publication [10] that this is due, in large part, to differences in the degree of discrimination in the various experiments against forward elastic scattering. Poor angular discrimination in the forward direction results in a smaller total scattering cross section due to the exclusion of regions of the angular scattering intensity. For the heavier rare gases this can be particularly important as the elastic DCS are significantly forward peaked at low energies, as a result of the large dipole polarizabilities of these atoms. Thus we believe that these differences result from the different levels of angular discrimination in the various experiments and a detailed discussion can be found in [10]. Whereas we have applied this correction to our

Table 2. Absolute grand total (σ_{GT}), grand total minus Ps formation (σ_{GT-Ps}) and Ps formation (σ_{Ps}) cross sections for Xe in units of 10^{-16} cm^2. Experimental uncertainties are as explained in the text.

Energy (eV)	σ_{GT}	σ_{GT-Ps}	σ_{Ps}
1.000	29.949	29.949	−0.350
2.000	21.561	21.561	−0.347
3.000	17.742	17.742	−0.157
4.000	16.451	16.451	−0.201
5.000	15.912	15.912	0.118
6.000	18.296	15.181	3.115
7.000	19.455	13.745	5.710
8.000	20.411	12.761	7.650
9.000	20.574	11.928	8.645
10.000	20.115	11.018	9.098
11.000	20.581	10.990	9.591
12.000	20.516	11.249	9.267
13.000	19.675	10.827	8.848
14.000	19.931	11.011	8.920
15.000	19.855	11.467	8.389
16.000	19.722	11.311	8.411
17.000	19.921	11.679	8.242
18.000	20.555	12.147	8.408
19.000	19.514	11.539	7.976
20.000	19.449	11.592	7.856
21.000	19.806	11.674	8.030
22.000	20.128	12.046	8.013
23.000	19.828	12.061	7.687
24.000	19.438	12.050	7.316
25.000	19.630	12.277	7.181
26.000	19.559	12.324	7.093
27.000	18.975	11.816	6.847
28.000	19.205	12.293	6.783
29.000	19.174	12.925	6.191
30.000	18.532	12.489	5.972
31.000	19.049	12.981	6.032
32.000	18.838	12.839	5.943
33.000	18.684	12.693	5.795
34.000	18.422	12.713	5.578
35.000	18.573	13.096	5.304
36.000	18.522	12.666	5.587
37.000	18.369	13.398	4.853
38.000	17.759	13.022	4.669
39.000	18.205	13.112	5.059
40.000	17.296	12.929	4.326
41.000	17.452	13.409	3.944
42.000	17.838	13.095	4.601
43.000	17.613	13.564	3.955
44.000	16.983	13.459	3.448

Table 2. Continued.

Energy (eV)	σ_{GT}	σ_{GT-Ps}	σ_{Ps}
45.000	17.131	13.178	3.885
46.000	17.398	13.644	3.470
47.000	16.871	13.488	3.361
48.000	17.240	13.494	3.424
49.000	16.654	13.506	2.975
50.000	16.388	13.357	2.894
51.000	16.433	13.661	2.679
52.000	16.715	13.787	2.836
53.000	16.618	14.067	2.467
54.000	16.431	13.857	2.522
55.000	16.642	14.215	2.276
56.000	16.532	14.117	2.207
57.000	15.947	13.956	1.942
58.000	16.139	13.997	1.988
59.000	16.176	14.512	1.569
60.000	15.588	13.613	1.705

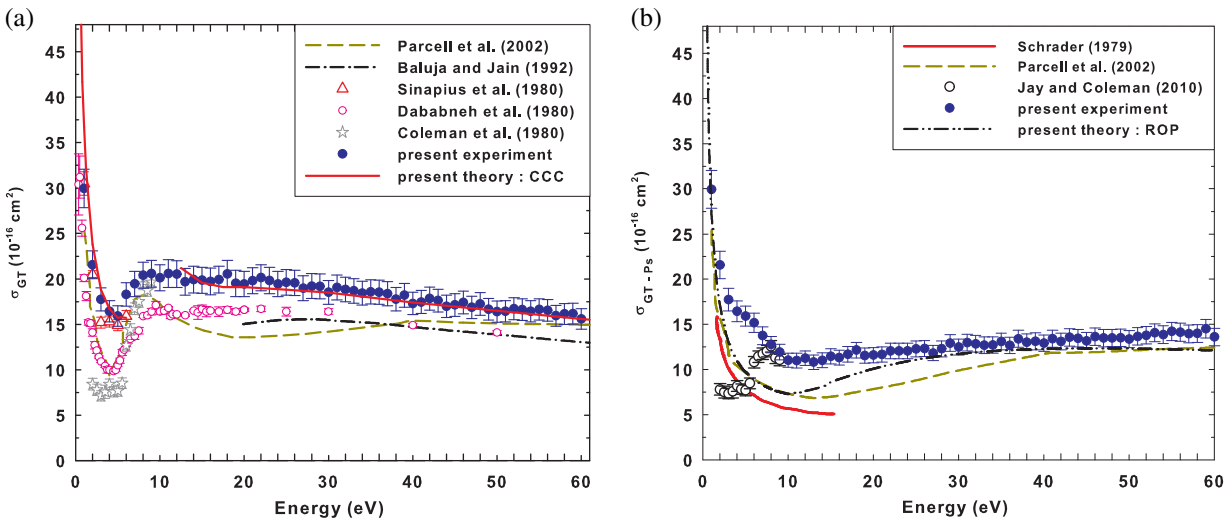

Figure 1. Positron scattering from Xe: (a) absolute total cross sections (σ_{GT}), in units of 10^{-16} cm^2; (b) absolute total minus Ps formation cross sections (σ_{GT}–σ_{Ps}), in units of 10^{-16} cm^2.

measured data, the other experiments have no correction applied for the angular discrimination, and if they did, their results would likely be much closer to ours.

The same figure 1(a) shows the comparison of the present experimental results with the results of three theoretical estimations, i.e. due to the present CCC, Baluja and Jain [12] and Parcell *et al* [13]. Good agreement is observed between the present experimental result and the present CCC calculation over the entire energy range, with the exception of the region between E_{Ps} (5.33 eV) and the ionization threshold E_{ion} at 12.13 eV. In this region we do not present

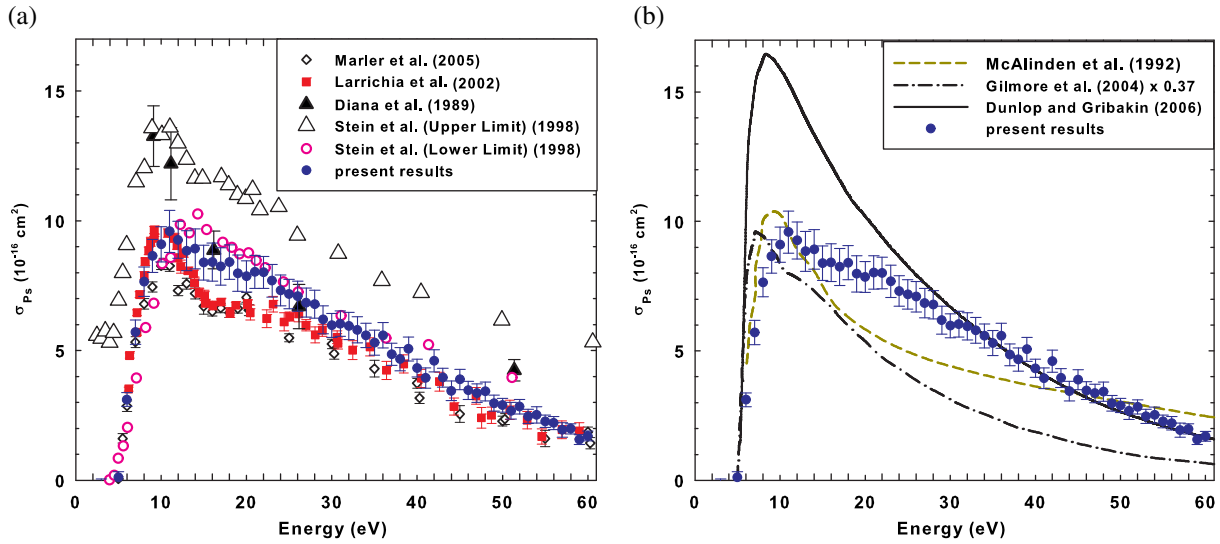

Figure 2. The present absolute total Ps formation cross sections (σ_{Ps}) for Xe, in units of 10^{-16} cm^2, compared with (a) previous experimental determinations and (b) various theoretical models.

calculated values from the CCC approach but merely join the value of the cross section at E_{Ps} with that at E_{ion} with a straight line to guide the eye. This issue highlights one of the problems that theory has in handling Ps formation in this energy region. In this region the presence of the Ps formation channel, leading also to ionization, requires a two-center expansion for accurate calculations. This problem has now been solved by new CCC formulations for helium [8], and work is ongoing to extend the two-center technique to the heavier noble gases. Good energy dependence agreement between the present experimental results and the earlier theoretical results of Baluja and Jain [12] is noted over the entire energy range of overlap. However, their calculated cross sections are lower in magnitude than the present experimental values by more than 25% across the entire energy range. With the exception of a similar energy dependence trend below E_{Ps}, the present cross section is neither in good qualitative agreement nor in quantitative agreement with the result of Parcell *et al* [13]. It is unclear why this is so, but it could be due in part to the fact that they did not explicitly calculate the total cross section, but rather derived it semi-analytically. Their paper was primarily concerned with calculating excitation cross sections. With these they combined their calculated elastic integral cross section and their ionization cross section (Campeanu *et al* [34]), and they used the Ps formation cross section from McAlinden and Walters [35] to derive the total cross section.

4.1.2. Grand total minus Ps formation cross section (σ_{GT}–σ_{Ps}). Figure 1(b) shows the current experimental and theoretical ROP results for σ_{GT}–σ_{Ps}, in comparison with the other results from the literature. Below the first excited state threshold for Xe (8.315 eV for positron impact) this channel is equivalent to the total elastic scattering channel. One reason for measuring this cross section is that it may be sensitive to channel coupling effects, which are possible between the elastic scattering channel and each, newly opening, inelastic channel. Such effects might be expected at or near the thresholds for Ps formation, electronic excitation and ionization. This has been the subject of a recent detailed study in our laboratory [36]. In that work, strong channel

coupling, manifesting itself as Wigner cusps, was observed in all of the rare gases at the Ps threshold. This manifests itself as the peak in the total elastic scattering cross section centered at 5.33 eV ($=E_{Ps}$), superimposed on a declining background but not seen in any of the other results shown in this figure. A difference is clearly observed with the only other experimental result, that of Jay and Coleman [37]. They observe a rise in σ_{GT}–σ_{Ps} above the Ps threshold, but the energy dependence and magnitude of their result are quite different from our measurements. This feature is observed neither in the current ROP calculation nor in the earlier calculation of Parcell *et al* [13], since neither approach explicitly treats Ps formation.

The result of Jay and Coleman [37] is not an absolute cross section but has been normalized to earlier experimental work, so while the present result is, for example, about 2.5 times larger at 3 eV, the significance of this is unclear. It may be that some of this difference is due to forward scattering effects that are not corrected for in their analysis. The two cross sections are in good agreement above 7.5 eV. Two theoretical results for σ_{GT}–σ_{Ps} from the literature [13, 38] and the present ROP calculations are also shown in figure 1(b). The present ROP result shows good qualitative agreement with the previous calculations of Parcell *et al* [13] and Schrader [38] below about 11 eV. Above this energy, qualitative and quantitative agreement is observed between the result of [13] and the present ROP cross section. While there is better general energy dependence and quantitative agreement between the present experimental and ROP results than with any of the other two earlier theories, there are also significant differences between the two results in the region between 1.5 and 20 eV, where the experimental cross section is as much as 30% higher than the theory.

4.1.3. Ps formation cross section (σ_{Ps}). In this section, the present experimental results for the total Ps formation cross section for Xe are discussed, in comparison with the experimental results from the literature in figure 2(a) and with theoretical results in figure 2(b).

As can be clearly seen in figures 2(a) and (b), there is a significant spread in the absolute magnitudes of both previous measurements and theoretical results for the Ps formation cross section. This lack of agreement has recently been discussed by Laricchia *et al* [39] and Marler *et al* [14]. One goal of the present work was to investigate these discrepancies. A detailed analysis of the various experimental techniques used for the previous measurements, and their strengths and weaknesses, has been carried out by both Laricchia *et al* and Marler *et al* and therefore not repeated here. The experimental technique used by Laricchia *et al* is that of measuring the total ion yield and then subtracting the direct ionization cross section they measured in an earlier experiment, to reveal the Ps formation cross section. Marler *et al* used a technique similar to the present one, where the Ps formation cross section is measured directly by monitoring positron loss in the scattering cell. Thus the significant disagreement observed between the present result and that of [14] in figure 2(a) was somewhat unexpected. One possible explanation, however, is that Marler *et al* use a single-scattering approximation in deriving σ_{Ps} in their work, whereas the present results are obtained by the use of the Beer–Lambert attenuation law, as has been fully discussed in [10]. To investigate the effect of this, we analyzed the present raw experimental data using the same technique as that of Marler *et al* and this accounts for approximately half, but not all, of the discrepancy seen in figure 2(a).

When comparing with previous measurements, we see that the level of agreement between the present experimental σ_{Ps} results and those of Diana *et al* [40] is poor, while better agreement is observed with the values corresponding to the lower limit (LL) results of Stein *et al* [41]. The former authors use a method whereby they measure the disappearance of the positrons in

the final state (a measure of all Ps formed), while the latter authors measured the simultaneous emission of two gamma rays coming from singlet (or para-) Ps and quenched triplet (or ortho-) Ps. In concept, the present technique of measuring the loss of positrons is similar to that used by Diana *et al.* The upper limit (UL) results of Stein *et al* were also measured using this same technique. However, these are larger than the present result over the entire energy range of overlap, e.g. about 30% larger at the peak in the cross section at about 10 eV.

There is close agreement, in both magnitude and energy dependence, between the results of Marler *et al* and Laricchia *et al*, except for the difference in magnitude over the peak region of the cross section, between 8 and 13 eV, where the latter is higher by about 20%. The present result shows better agreement with the Laricchia *et al* values, qualitatively and quantitatively, over the energy range from E_{Ps} until above the peak energy at about 13 eV. It is, however, different from the result of Laricchia *et al* above this energy. One of the differences that is worth noting is that Laricchia *et al* reported a second peak in σ_{Ps} that is not observed in the present result, and this has been discussed by Marler *et al*.

In figure 2(b), we compare the present measurements and the three theoretical results available from the literature, two of which are coupled channel calculations [15, 34] and one a many-body theory approach [42]. This comparison reveals generally good agreement in the energy dependence of the Ps formation cross section. However, there are significant quantitative differences observed between the present experimental result and all of the three theoretical cross sections, in particular the result of Gilmore *et al* [15]. All three theoretical results show a rather sharp peak in the cross section at about 7–9 eV, whereas the present experimental result shows a rather broad peak spanning the energy range of 8–20 eV. In addition, all three theories predict a larger σ_{Ps} than experiment below 11 eV, with the difference being up to 50% in the case of the calculation of Dunlop and Gribakin [42]. Good agreement, however, is observed between the present results and this calculation at energies above 30 eV. It is interesting to note that the differences compared with these three theories, and the agreement with the result of [42] at higher energies, are very similar to the observations made in our earlier study of σ_{Ps} for Kr [11].

4.2. Elastic differential cross sections

The present experimental and theoretical elastic DCS results are shown in figures 3–5, where they are also compared with the relatively scarce results available in the literature. The present theoretical results represent values obtained using both the CCC and the ROP methods. It is worth noting that the results of Kauppila *et al* [17] presented in figures 3 and 4, for energies 5, 10 and 20 eV, have been folded about 90° to enable comparison with the present data (see section 2.2). In addition, as their values were relative cross sections, they have been normalized to the present data at 30°. It is also worth noting that to obtain the absolute values that they published, Kaupilla *et al* normalized their data to the non-relativistic polarized orbital calculation of [18].

Figures 3(a)–(d) show the present elastic DCS results for energies 1, 2, 5 and 8 eV, respectively. These are compared with the other absolute experimental data available in the literature, at several energies, namely from Marler *et al* [16] whose experimental technique was similar to the present. Also shown at 5 eV is the relative measurement of Kaupilla *et al* [17]. In addition to the present calculations, we also show theoretical cross sections by Sin Fai Lam [19] for 1, 2 and 8 eV. A common feature of the DCS for all these energies, as indicated in all four panels of figure 3, is that they all rise sharply in the forward direction towards the 0° scattering

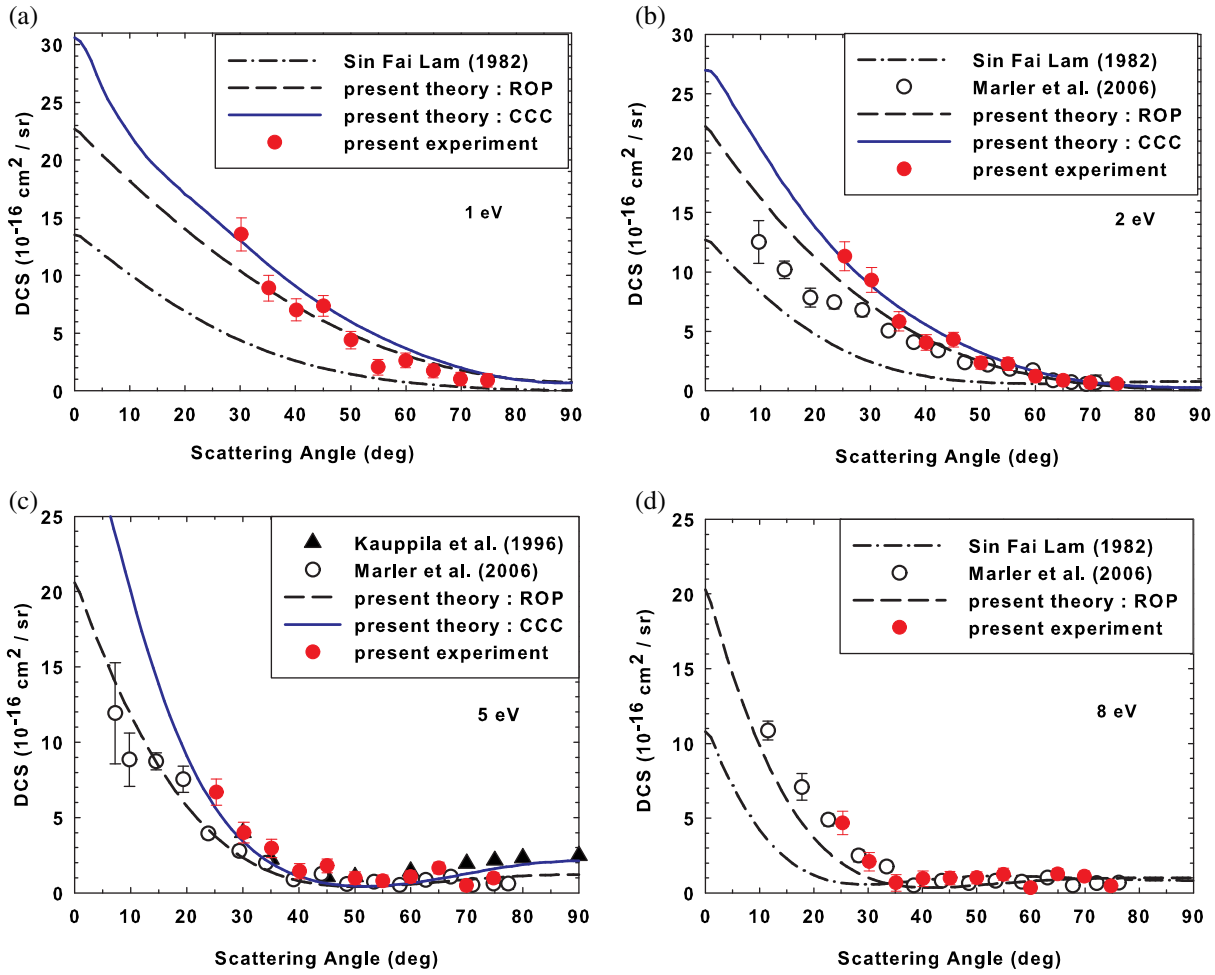

Figure 3. Absolute elastic DCS (10^{-16} cm^2 sr^{-1}) for positron scattering from Xe compared with experimental and theoretical values from the literature at energies from 1 to 8 eV.

angle. This is due to the relatively large atomic dipole polarizability of Xe, which results in enhanced long-range interactions and stronger forward angle scattering at these energies.

There is good quantitative agreement between the present experimental results and those of Marler *et al* at all common scattering angles for 8 eV and above 35° for 2 and 5 eV. Good qualitative agreement is observed between the present experimental result and the data of Kaupilla *et al* at 5 eV. The subtle differences observed between the two present theoretical results, below 15° at 1 and 2 eV, and below 35° at 5 eV, are thought to be due to differences in the way in which the polarization interaction is treated. The theoretical results of Sin Fai Lam [19] underestimate the amount of forward scattering at all the energies shown in these panels. These results were obtained using the Pople–Schofield approximation for the dipole polarization potential. Our ROP calculations, for example, include the dipole and the next four higher multipole polarization potentials. Increasing the number of multipoles increases the cross section at all angles, compared with the case of using only the dipole. This, in part, may explain some of the differences observed between our results and those of Sin Fai Lam at forward

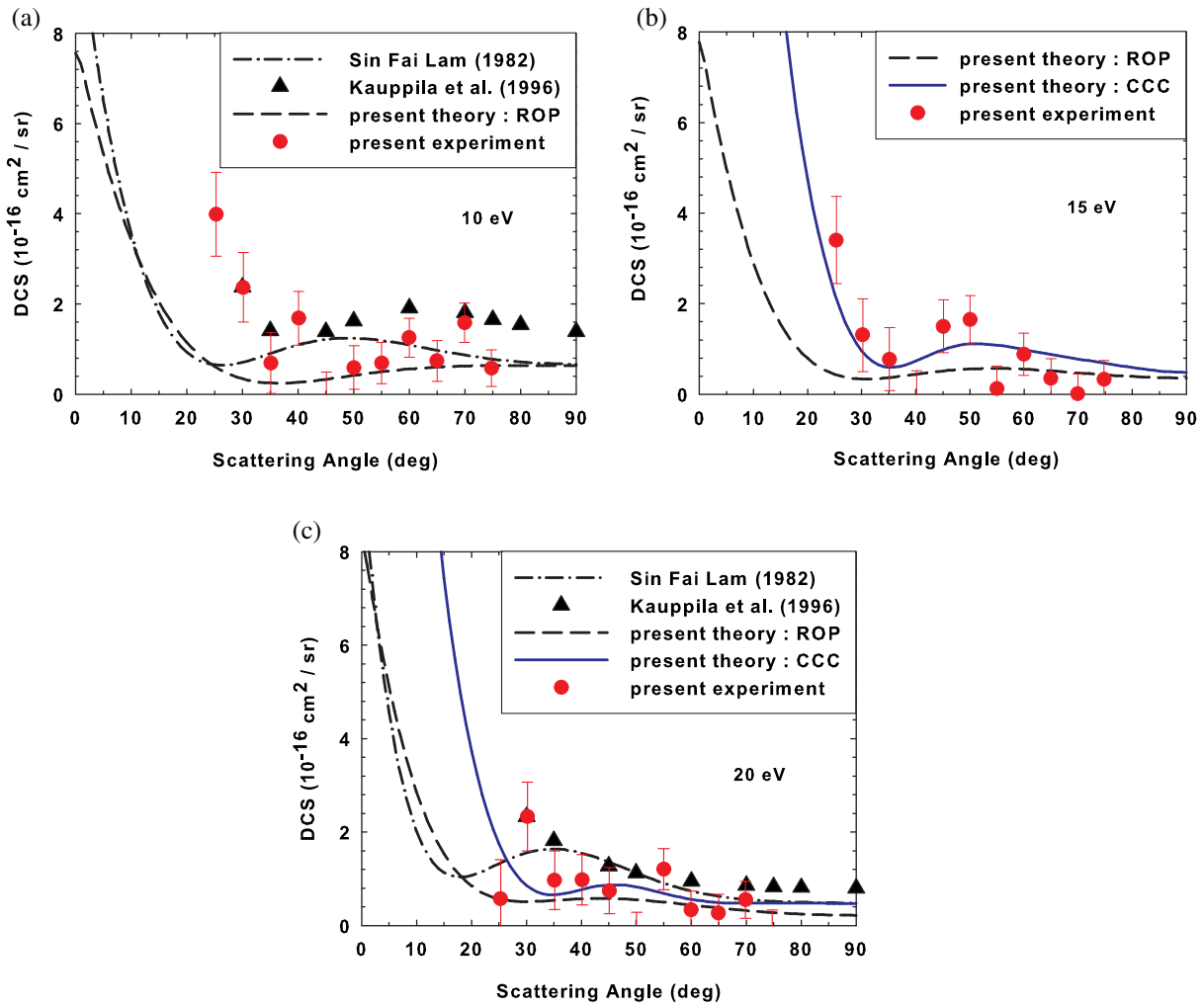

Figure 4. The same as figure 3 but for energies from 10 to 20 eV.

angles. At 1 and 2 eV, there is generally good qualitative and quantitative agreement between the present experimental results and theoretical results. The present experimental data for 5 eV are in better agreement with the CCC results than the ROP, especially in regard to the extent of forward scattering. Good agreement is observed between the present experimental and ROP results at 8 eV, except for the subtle magnitude differences below 35°.

Figures 4(a)–(c) show the present elastic DCS results for the energies of 10, 15 and 20 eV, respectively, in comparison with the values from the literature. The agreement between the present experimental data and that of [17] is reasonably good over the angular range of overlap for 10 and 20 eV. Although they show a similar angular dependence, the results from the two theoretical approximations shown in panels (b) and (c) differ significantly in magnitude at angles below 35°. Above this angle however, the two theoretical results are in close agreement with each other as well as with the present experimental values. This difference in magnitude between the ROP and the CCC below 35° is most likely attributable either to differences in handling the polarization potentials by these two methods or to the fact that the CCC includes Ps formation, which has a significant effect on the shape of the low-angle elastic DCS. At 15 eV (panel (b)),

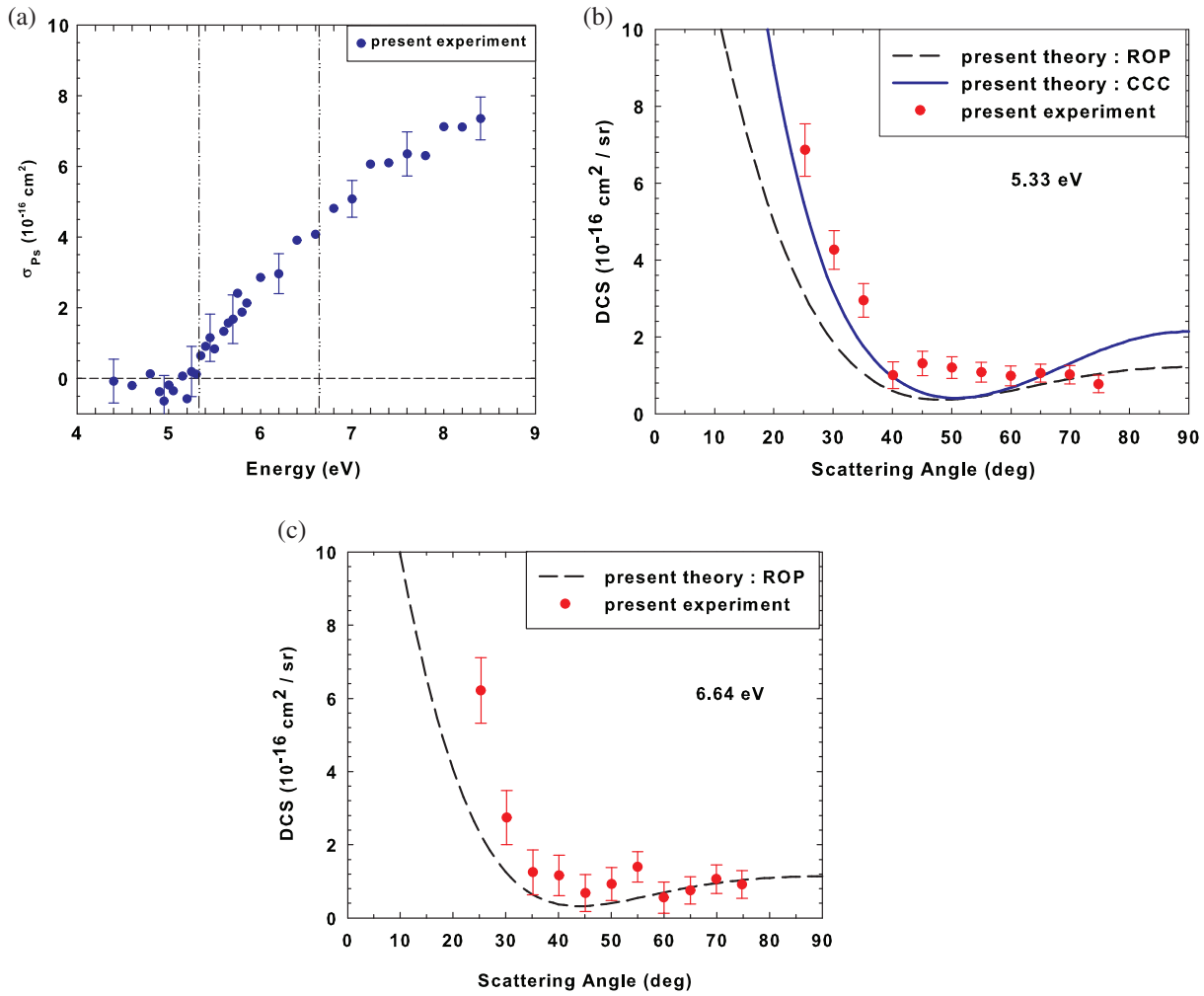

Figure 5. (a) The same as figure 2 but at finer energy steps over the energy region 4.4–8.4 eV; (b, c) the same as figure 3 but at the Ps formation threshold energies 5.33–6.64 eV. The vertical dash-dot-dot-dash lines in panel (a) show the positions of the energies 5.33–6.64 eV.

the CCC agrees better with the current experimental result, especially with regard to the extent of forward scattering. The results of Sin Fai Lam [19] shown in panels (a) and (c) are in better agreement with the present ROP values, compared with the data in figure 3, except for the angular ranges 25°–80° for 10 eV (panel (a)) and 20°–70° for 20 eV (panel(c)) where the former shows a peak feature, which is not observed in the latter cross section.

4.3. Investigation at the fine-structure thresholds of the Xe^+ *ion*

When a positron interacts with a Xe atom, it can detach an electron in a process of single ionization, leading to the formation of the Xe^+ ion. The first ionization potential (IP) for this process is 12.13 eV, resulting in a Ps threshold (E_{Ps}) of 5.33 eV for Xe. However, the ground state of the Xe^+ ion is split by the spin–orbit interaction, and the fine-structure components ($^2P_{3/2}$, $^2P_{1/2}$) are split in energy by 1.307 eV [43]. Thus, the threshold for ionization that leaves

the ion in the $^2P_{1/2}$ state is 13.41 eV. It follows that another Ps threshold, associated with this ion core state might be expected at an energy equal to 5.33 + 1.307 eV, or ~6.64 eV. It also follows that one might possibly expect to see the effect of the opening of this Ps formation channel in the total Ps formation cross section. We have investigated, experimentally and theoretically, this possibility, by carrying out fine energy step measurements of σ_{Ps} over the limited energy range of 4.4–8.4 eV, as well as measuring elastic DCS at the two threshold energies of 5.33 and 6.64 eV.

Figure 5(a) shows the σ_{Ps} for Xe over this energy range covering the two threshold energies. Indeed the initial rise of this cross section from zero coincides with the first E_{Ps} at 5.33 eV, which is an important confirmation of the energy scale calibration based on the RPA cut-off position. However, there is no clear evidence of any visible feature, or change of slope in the cross section, corresponding to the expected second E_{Ps} at 6.64 eV. That there is no observable effect at the threshold possibly indicates that the $J = 1/2$ contribution turns on slowly (as does the $J = 3/2$), and is most likely smaller.

Figures 5(b) and (c) show the present elastic DCS results at the two threshold energies, 5.33 and 6.64 eV. The experimental results in these plots show no particular features that would differentiate them from those measured at the nearest energies of 5 and 8 eV. The ROP and CCC results show the same energy dependence as the experimental values at 5 eV, although, out of the two theoretical approximations, the CCC shows better agreement with the experimental data, especially with respect to the extent of forward scattering. At 6.64 eV, only the ROP result shows the same energy dependence as the experimental data over the entire angular range of overlap. The CCC deviates from both the experimental and ROP energy dependences by indicating a small peak between 35° and 85°. It must be noted, however, that the CCC result is most likely inaccurate, as this is in the energy region between E_{Ps} and E_{ion} where the multicentered approach discussed earlier is clearly required.

5. Conclusion

In this paper we have presented absolute experimental measurements of the grand total, total Ps formation and total elastic cross sections for positron scattering from Xe at energies from 1 to 60 eV. The CCC and ROP approaches have been used to calculate the σ_{GT} and σ_{GT}–σ_{Ps} cross sections, respectively. These data are compared with experimental and theoretical calculations from the literature, among which there existed significant differences, for all three cross sections. Absolute measurements of the elastic DCS have also been carried out, together with theoretical computations of these cross sections using our two techniques for energies of 1, 2, 5, 8, 9, 10, 15 and 20 eV. By carrying out finer energy step measurements of the Ps formation cross section over the energy range of 4.4–8.4 eV and elastic DCS at the energies of 5.33 and 6.64 eV, we have also investigated the energy region of the Ps thresholds for the two ground state components ($^2P_{3/2}$, $^2P_{1/2}$) states of the Xe^+ ion, and found no evidence of any second Ps formation threshold features at 6.64 eV.

Acknowledgments

The authors acknowledge funding from the Centre of Excellence Program of the Australian Research Council (ARC). CM is also grateful to the ARC for financial support under the Australian Postdoctoral Fellowships program. We also thank the technical staff at the Australian

National University, namely Graeme Cornish, Stephen Battisson, Ross Tranter and Ron Cruikshank, for their invaluable input.

References

[1] Zatsarinny O and Bartschat K 2010 *J. Phys. B: At. Mol. Opt. Phys.* **43** 074031
[2] Buckman S J and Sullivan J P 2006 *Nucl. Instrum. Methods* B **247** 5
[3] Gilbert S J, Kurz C, Greaves R G and Surko C M 1997 *Appl. Phys. Lett.* **70** 1944
[4] Gilbert S J, Greaves R G and Surko C M 1999 *Phys. Rev. Lett.* **82** 5032
[5] Sullivan J P, Gilbert S J, Marler J P, Greaves R G, Buckman S J and Surko C M 2002 *Phys. Rev.* A **66** 042708
[6] Sullivan J P, Makochekanwa C, Jones A, Caradonna P and Buckman S J 2008 *J. Phys. B: At. Mol. Opt. Phys.* **41** 081001
[7] Caradonna P, Jones A, Makochekanwa C, Slaughter D S, Sullivan J P, Buckman S J, Bray I and Fursa D V 2009 *Phys. Rev.* A **80** 032710
[8] Utamuratov R, Kadyrov A S, Fursa D V, Bray I and Stelbovics A T 2010 *J. Phys. B: At. Mol. Opt. Phys.* **43** 125203
[9] Caradonna P, Sullivan J P, Jones A, Makochekanwa C, Slaughter D, Mueller D W and Buckman S J 2009 *Phys. Rev.* A **80** 060701
[10] Jones A C L 2011 *Phys. Rev.* A **83** 032701
[11] Makochekanwa C 2011 *Phys. Rev.* A **83** 032721
[12] Baluja K L and Jain A 1992 *Phys. Rev.* A **46** 1279
[13] Parcell L A, McEachran R P and Stauffer A D 2002 *Nucl. Instrum. Methods* B **192** 180
[14] Marler J P, Sullivan J P and Surko C M 2005 *Phys. Rev.* A **71** 022701
[15] Gilmore S, Blackwood J E and Walters H R J 2004 *Nucl. Instrum. Methods* B **221** 129
[16] Marler J P, Surko C M, McEachran R P and Stauffer A D 2006 *Phys. Rev.* A **73** 064702
[17] Kaupilla W E, Kwan C K, Przybyla D, Smith S J and Stein T S 1996 *Can. J. Phys.* **74** 474
[18] McEachran R P, Stauffer A D and Campbell L E M 1980 *J. Phys. B: At. Mol. Opt. Phys.* **13** 1281
[19] Sin Fai Lam L T 1982 *J. Phys. B: At. Mol. Opt. Phys.* **15** 143
[20] Sullivan J P, Jones A, Caradonna P, Makochekanwa C and Buckman S J 2008 *Rev. Sci. Instrum.* **79** 113105
[21] Sullivan J P, Makochekanwa C, Jones A, Caradonna P, Slaughter D S, Machacek J R, McEachran R P, Mueller D W and Buckman S J J 2011 *J. Phys. B: At. Mol. Opt. Phys.* **44** 035201
[22] Sullivan J P, Jones A, Caradonna P, Makochekanwa C and Buckman S J 2008 *Nucl. Instrum. Methods* B **266** 384
[23] Chen S, McEachran R P and Stauffer A D 2008 *J. Phys. B: At. Mol. Opt. Phys,* **41** 025201
[24] Utamuratov R, Kadyrov A S, Fursa D V, Bray I and Stelbovics A T 2010 *J. Phys. B: At. Mol. Opt. Phys.* **43** 125203
[25] Grant I P, McKenzie B J, Norrington P H, Mayers D F and Pyper N C 1980 *Comput. Phys. Commun.* **21** 207
[26] Bray I and Stelbovics A T 1992 *Phys. Rev.* A **46** 6995
[27] Bray I and Stelbovics A T 1993 *Phys. Rev.* A **48** 4787
[28] Wu H, Bray I, Fursa D V and Stelbovics A T 2004 *J. Phys. B: At. Mol. Opt. Phys,* **37** L1
[29] Fursa D V and Bray I 1997 *J. Phys. B: At. Mol. Opt. Phys.* **30** 5895
[30] Kumar A and Meath W 1985 *Can. J. Chem.* **63** 1616
[31] Sinapius G, Raith W and Wilson W G 1980 *J. Phys. B: At. Mol. Opt. Phys.* **13** 4079
[32] Coleman P G, McNutt J D, Diana L M and Hutton J T 1980 *Phys. Rev.* A **22** 2290
[33] Dababneh M S, Kauppila W E, Downing J P, Laperriere F, Pol V, Smart J H and Stein T S 1980 *Phys. Rev.* A **22** 1872
[34] Campeanu R I, McEachran R P and Stauffer A D 2002 *Nucl. Instrum. Methods* B **192** 146
[35] McAlinden M T and Walters H R J 1992 *Hyperfine Interact.* **73** 65

[36] Jones A C L, Caradonna P, Makochekanwa C, Slaughter D S, McEachran R P, Machacek J R, Sullivan J P and Buckman S J 2010 *Phys. Rev. Lett.* **105** 073201
[37] Jay P M and Coleman P G 2010 *Phys. Rev.* A **82** 012701
[38] Schrader D M 1979 *Phys. Rev.* A **20** 918
[39] Laricchia G, Van Reeth P, Szluinska M and Moxom J 2002 *J. Phys. B: At. Mol. Opt. Phys.* **35** 2525
[40] Diana L M *et al* 1989 *Positron Annihilation* ed L Dorokins-Vanpraet, M Dorokins and D Segers (Singapore: World Scientific) p 311
[41] Stein T S, Harte M, Jiang J, Kauppila W E, Kwan C K, Li H and Zhou S 1998 *Nucl. Instrum. Methods* B **143** 68
[42] Dunlop L J M and Gribakin G F 2006 *Nucl. Instrum. Methods* B **247** 61
[43] Moore C E 1971 *Atomic Energy Levels' National Standards Reference Data System* (Washington, DC: US Govt Printing Office)